Variational Assimilation of GOME Total-Column Ozone Satellite Data in a 2D Latitude–Longitude Tracer-Transport Model

H. J. ESKES, A. J. M. PITERS, P. F. LEVELT, M. A. F. ALLAART, AND H. M. KELDER

Royal Netherlands Meteorological Institute, De Bilt, Netherlands

(Manuscript received 29 June 1998, in final form 22 December 1998)

ABSTRACT

A four-dimensional data-assimilation method is described to derive synoptic ozone fields from total-column ozone satellite measurements. The ozone columns are advected by a 2D tracer-transport model, using ECMWF wind fields at a single pressure level. Special attention is paid to the modeling of the forecast error covariance and quality control. The temporal and spatial dependence of the forecast error is taken into account, resulting in a global error field at any instant in time that provides a local estimate of the accuracy of the assimilated field. The authors discuss the advantages of the 4D-variational (4D-Var) approach over sequential assimilation schemes. One of the attractive features of the 4D-Var technique is its ability to incorporate measurements at later times $t > t_0$ in the analysis at time t_0, in a way consistent with the time evolution as described by the model. This significantly improves the offline analyzed ozone fields.

1. Introduction

Data assimilation is an essential tool in numerical weather prediction, which depends on an accurate analysis of the present state of the atmosphere. In climate and atmospheric chemistry research, however, the interest in data assimilation is more recent, related to the increasing availability of satellite data for chemical species. Combining measurements and models by means of data assimilation provides an estimate of the state of the atmosphere at any position and time within the resolution of the model. It serves as a tool to test atmospheric models and to validate the measurements.

Modern data-assimilation schemes like four-dimensional variational assimilation (4D-Var) (Lewis and Derber 1985; Le Dimet and Talagrand 1986) and Kalman filtering (Jazwinski 1970) have interesting additional properties due to the explicit appearance of the model in the analysis equations. In atmospheric chemistry modeling the observation of certain chemical species (e.g., O_3, NO_2) can result in a balanced time and space distribution of others (e.g., NO, N_2O_5, etc.) due to the explicit chemical equations in the 4D-Var analysis (see Fisher and Lary 1995; Elbern et al. 1997). Another example is the combination of a global circulation model, ozone measurements, and a 4D-Var assimilation scheme. The additional ozone data may lead to an improved description of the wind in the lower stratosphere (e.g., Riishøjgaard 1996).

In this paper the advantages of the 4D-Var assimilation method to derive global tracer fields will be investigated. A detailed forecast error estimation approach is introduced. Ozone is transported by a simple and practical global 2D (lat–long) advection model (Levelt et al. 1996) using European Centre for Medium-Range Weather Forecasts (ECMWF) wind fields. As input data we use retrieved total ozone from the Global Ozone Monitoring Experiment (GOME) spectrometer (Burrows 1993).

The swath of the GOME instruments is relatively narrow (960 km), and a global coverage is obtained in about three days. The observed ozone distribution shows strong variations on large and small scales, and these structures are transported by the wind over several thousands of kilometers in this period. The sparseness of the data, the large ozone fluctuations, and the transport suggest the usefulness of combining the measurements with a tracer-transport model by means of data assimilation. This will fill the spatial and temporal gaps in the data and provide (almost) global ozone distributions at any moment required.

The maximum knowledge of the ozone distribution will be obtained when truly three-dimensional measurements are combined with a 3D model. GOME is a unique instrument, combining the good horizontal resolution of nadir viewing instruments with a high spectral resolution of 0.2–0.4 nm over a broad spectral range in the UV and visible, from 240 to 790 nm. This spectral data can be inverted in order to obtain detailed height-

Corresponding author address: Dr. H. J. Eskes, KNMI, P.O. Box 201, 3730 AE, De Bilt, Netherlands.
E-mail: eskes@knmi.nl

resolved ozone information, including the troposphere (Munro et al. 1998; Eichmann et al. 1997). However, at present the retrieval of ozone profiles from the spectra is time consuming and the main real-time GOME product consists of total columns of ozone. Furthermore, the important Total Ozone Mapping Spectrometer (TOMS) instruments from National Aeronautics and Space Administration (NASA) and the Television Infrared Observation Satellite (TIROS) Operational Vertical Sounder instruments from the National Oceanic and Atmospheric Administration also deliver vertically integrated ozone fields. A practical tool to assimilate ozone *column* measurements is useful, given this abundance of total ozone data.

The assimilation of total ozone in a 3D model is hampered by a lack of information. At what altitude should the ozone be inserted in the model, or, how should the vertically integrated mismatch between model and measurement be distributed over the vertical model layers? Uncertainties in the vertical covariances lead to corresponding uncertainties in the quality of the model profiles. Unfortunately there is not much experimental data from which to obtain the required vertical error statistics. Nadir satellite instruments are theoretically limited to a vertical resolution of 5–8 km. Limb instruments reach a resolution of about 1 km, but the horizontal resolution is much worse. Ozone sondes are very sparse and the quality is often difficult to judge. Different strategies to model the vertical ozone distribution have been introduced (Riishøjgaard et al. 1992; Lary et al. 1995; Jeuken et al. 1999). In this paper this profile problem will be circumvented by using the advection equation in a two-dimensional model. The 2D model, fed with 2D observations, allows a direct estimate of the forecast error covariance. The model is simple and runs with a relatively high resolution of about 100 × 100 km with only limited computer demands. This grid-cell area is comparable to the area of a GOME ground pixel. On the other hand, the 2D approach is a considerable simplification of the 3D transport in the atmosphere, and model errors will correspondingly be larger than in a proper 3D general circulation model.

The 2D assimilation model KNMI (AMK) was discussed in a previous paper by Levelt et al. (1996). The assimilation model discussed here contains several adjustments compared to the original AMK. The 4D variational assimilation replaces the original single-correction scheme. The program now uses a semi-Lagrangian advection, instead of the original upwind formulation. An important prerequisite for an assimilation tool is a realistic estimate of the forecast error distribution. Therefore, a considerable part of this paper is devoted to covariance modeling.

In the next section the 4D-Var assimilation scheme and several implementation aspects are explained. Section 3 discusses the GOME ozone observations. The advection model is discussed in section 4. The forecast error covariance is constructed out of a homogeneous and isotropic correlation function and a local error field. These two ingredients and the forecast and correlation statistics are described in section 5. The paper is concluded by discussing the results of the assimilation of GOME ozone columns with the 4D-Var approach.

2. Four-dimensional variational assimilation

In data-assimilation schemes like optimal interpolation or successive correction, data are analyzed at given instants in time and only the spatial distribution of measurements is taken into account. This implies that the model, describing the time evolution of the system, does not have a direct influence on the error covariances, and the relation between observations at different analysis times is not properly accounted for. In four-dimensional variational assimilation and Kalman filtering, however, the model is an active ingredient of the analysis scheme. In 4D-Var a time interval $t \in [0, T]$ is chosen, and all the data in this interval is incorporated in a single analysis. The covariance matrix acquires a flow-dependent component on the interval $[0, T]$, leading to an additional coupling between the field variables that is consistent with the dynamics as specified by the model.

The optimal analysis field (assuming Gaussian error statistics) is the tracer (ozone) field $\mathbf{x}$ that minimizes the cost or penalty function J (Daley 1991; Lewis and Derber 1985; Le Dimet and Talagrand 1986; Talagrand and Courtier 1987; Lorenc 1988; Courtier et al. 1993):

$$J[\mathbf{x}_0, \mathbf{x}_1, \cdots \mathbf{x}_T] = \frac{1}{2}\sum_{m,n}^{M} (\mathbf{H}_m \mathbf{x}_{t_m} - y_m)(\mathbf{O}^{-1})_{m,n}(\mathbf{H}_n \mathbf{x}_{t_n} - y_n) + \frac{1}{2}(\mathbf{x}_0 - \mathbf{x}^b)^{\mathrm{T}}\mathbf{B}^{-1}(\mathbf{x}_0 - \mathbf{x}^b). \quad (1)$$

The vector $\mathbf{x}_t$ is a list of all model variables at time t (total ozone values at every grid point), which are the ozone total-column values in our case. Here M is the number of measurements in the interval. The observation operator $\mathbf{H}_m$ calculates a prediction for measurement m using the model field at time t_m (see also section 3). Since the field has to be known at all measurement times, J is, in principle, a function in a space with a very large dimension equal to the number of model variables (ozone values) times the number of time steps in the interval $[0, T]$. The innovation numbers $(\mathbf{H}_m \mathbf{x}_{t_m} - y_m)$ quantify the mismatch between model and measurements. The quadratic form of J is related to the assumption that the errors are distributed in a Gaussian way. The matrix $\mathbf{O}$ is a combined instrument, retrieval, and representativeness error covariance:

$$O_{m,n} = \langle (\mathbf{H}_m \mathbf{x}^t_{t_m} - y_m)(\mathbf{H}_n \mathbf{x}^t_{t_n} - y_n) \rangle, \quad (2)$$

where $\mathbf{x}^t$ represents the unknown true field values on the model grid. The model ozone values are interpreted as the average ozone column in the corresponding model grid cell. Similarly the GOME total ozone is an average over the footprint of the instruments. These two areas

are not identical and this introduces a representativeness mismatch between the model and the observation. The last term in Eq. (1) measures the difference between the field $\mathbf{x}$ and the first guess field $\mathbf{x}^b$ at time $t = 0$. This field $\mathbf{x}^b$ will normally be the result of the analysis at the end of the previous time interval, $[-T, 0]$. The covariance matrix $\mathbf{B} = \langle(\mathbf{x}^b - \mathbf{x}^t)(\mathbf{x}^b - \mathbf{x}^t)^{\mathrm{T}}\rangle$.

The time evolution of the field $\mathbf{x}_t$ is described by the 2D advection model M:

$$\mathbf{x}_t = \mathbf{M}[\mathbf{x}_{t-1}] = \mathbf{M}[\mathbf{M}[\cdots\mathbf{M}[\mathbf{x}_0]]]. \tag{3}$$

Note that the model $\mathbf{M}$ is a function of time since the wind field is updated every time step. All future times are now fully determined by the field at time $t = 0$. By means of this deterministic relation the dimension of the control variable $\mathbf{x}_0 \cdots \mathbf{x}_T$ of J is reduced considerably, and the cost is only a function of the start field $\mathbf{x}_0$. Eq. (3) represents a strong constraint: model errors are not taken into account explicitly in the interval $t = [0, T]$ and a model error term is not included in the cost function Eq. (1). This simplification is usually made in 4D-Var and we also use it in the derivation below. However, the model error, accumulated over the interval $[0, T]$, will result in a contribution to the forecast error covariance at time T, the matrix $\mathbf{B}$ for the next interval $[T, 2T]$. This will be discussed further in section 5.

To minimize J in an efficient way it is necessary to compute its gradient. Consider a small incremental field $\Delta\mathbf{x}$. The model $\mathbf{M}$ can now be linearized around a reference trajectory $\mathbf{x}_t$:

$$\mathbf{x}_{t+1} + \Delta\mathbf{x}_{t+1} = \mathbf{M}[\mathbf{x}_t + \Delta\mathbf{x}_t] \approx \mathbf{M}[\mathbf{x}_t] + \frac{d\mathbf{M}}{d\mathbf{x}}\Delta\mathbf{x}_t$$
$$= \mathbf{M}[\mathbf{x}_t] + \mathbf{L}(\mathbf{x}_t)\Delta\mathbf{x}_t. \tag{4}$$

The matrix $\mathbf{L}$ consists of the derivatives of the vector operator $\mathbf{M}$ with respect to the model variables $\mathbf{x}$. When the model is nonlinear, the matrix elements of $\mathbf{L}$ still depend on the field values $\mathbf{x}_t$. The departure $\Delta\mathbf{x}$ leads to a small increase in the cost:

$$\Delta J = J(\mathbf{x}_0 + \Delta\mathbf{x}_0) - J(\mathbf{x}_0)$$
$$\approx \sum_{m,n}^{M} (\mathbf{H}_m\mathbf{x}_{t_m} - y_m)^{\mathrm{T}}O_{m,n}^{-1}\mathbf{H}_n\Delta\mathbf{x}_{t_n} + (\mathbf{x}_0 - \mathbf{x}^b)^{\mathrm{T}}\mathbf{B}^{-1}\Delta\mathbf{x}_0$$
$$= \nabla J(\mathbf{x}_0)^{\mathrm{T}} \cdot \Delta\mathbf{x}_0. \tag{5}$$

This increase in J is, by definition, equal to the inner product of the gradient of J, ∇J, and the field increment $\Delta\mathbf{x}_0$. Inserting Eq. (4) in Eq. (3) gives

$$\Delta\mathbf{x}_t = \mathbf{L}(\mathbf{x}_{t-1}) \cdots \mathbf{L}(\mathbf{x}_0)\Delta\mathbf{x}_0. \tag{6}$$

The gradient of the cost function is therefore

$$\nabla J(\mathbf{x}_0) = \sum_{m,n}^{M} \mathbf{L}^{\mathrm{T}}(\mathbf{x}_0)\mathbf{L}^{\mathrm{T}}(\mathbf{x}_1) \cdots \mathbf{L}^{\mathrm{T}}(\mathbf{x}_{t_n-1})\mathbf{H}_n^{\mathrm{T}}$$
$$\times O_{m,n}^{-1}(\mathbf{H}_n\mathbf{x}_{t_n} - y_n) + \mathbf{B}^{-1}(\mathbf{x}_0 - \mathbf{x}^b). \tag{7}$$

Note that the fields $\mathbf{x}_1$ to $\mathbf{x}_{t_n-1}$ are computed from Eq. (3), and therefore ∇J is a function of $\mathbf{x}_0$ only. The transpose $\mathbf{L}^{\mathrm{T}}$ of the linear forward model is called the adjoint model.

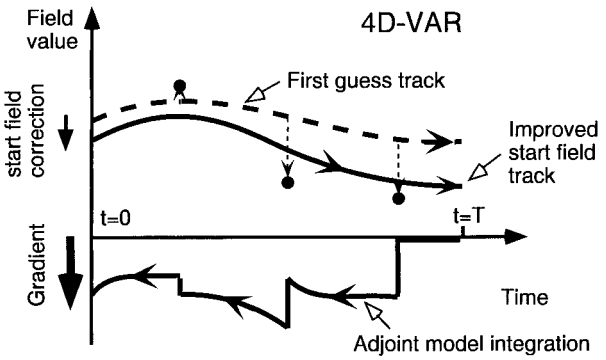

FIG. 1. The 4D-Var assimilation process. A first-guess field at time $t = 0$ is integrated forward in time (dashed line), and the differences (vertical arrows) between the measurements (dots) and the model are recorded. The adjoint field is set to zero at time T and then advanced backward in time using the linear adjoint model $\mathbf{L}^{\mathrm{T}}$. At the measurement times the innovations are added (jumps). Reaching time $t = 0$ the background term [see Eq. (7)] is added to the adjoint, resulting in the gradient of the cost function. Using this gradient a new improved start field is constructed, and the cycle is repeated until convergence is reached.

Given the cost function and its gradient, a minimization routine can be used to approach the minimum, equivalent to the analyzed field $\mathbf{x}^a$. We used the quasi-Newton routine m1qn3 (Gilbert and Lemaréchal 1989). The 4D-Var data-assimilation process is summarized in Fig. 1. As time interval we take $T = 24$ h; see next section.

Instead of the ozone field $\mathbf{x}$, also a monotonically increasing function $\mathbf{w}(\mathbf{x})$ may be used as control variable in the minimization. This ''preconditioning'' does not change the minimum of the cost function, but it can have a considerable effect on the convergence of the iteration process. As will be described in the next sections, we write the covariance matrix as a product of a diagonal variance field $\mathbf{D}$ and a homogeneous correlation matrix $\mathbf{F} = \mathbf{A}^2$, $\mathbf{B} = \mathbf{ADA}$. Various choices for the control variable $\mathbf{w}$ were tested, and the best convergence was obtained using $\mathbf{w} = \mathbf{A}^{-1}(\mathbf{x}_0 - \mathbf{x}^b)$. In this case the cost function and its gradient become

$$J[\mathbf{w}] = \frac{1}{2}\sum_{m,n}^{M} (\mathbf{H}_m\mathbf{x}_{t_m} - y_m)^{\mathrm{T}}O_{m,n}^{-1}(\mathbf{H}_n\mathbf{x}_{t_n} - y_n)$$
$$+ \frac{1}{2}\mathbf{w}^{\mathrm{T}}\mathbf{D}^{-1}\mathbf{w},$$
$$\mathbf{x}_0 = \mathbf{x}_b + \mathbf{Aw}. \tag{8}$$

$$\nabla J(\mathbf{x}_0) = \mathbf{A}^{\mathrm{T}}\sum_{m,n}^{M} \mathbf{L}^{\mathrm{T}}(\mathbf{x}_0) \cdots \mathbf{L}^{\mathrm{T}}(\mathbf{x}_{t_n-1})\mathbf{H}_n^{\mathrm{T}}$$
$$\times O_{m,n}^{-1}(\mathbf{H}_n\mathbf{x}_{t_n} - y_n) + \mathbf{D}^{-1}\mathbf{w}. \tag{9}$$

This choice can be understood in the following way.

The measured innovation numbers give rise to local corrections and, therefore, the adjoint field in Eq. (7) contains large amplitudes at high wavenumbers. In the next iteration the cost function [Eq. (1)] is evaluated, and the inverse background matrix $\mathbf{B}^{-1}$ will add large contributions to J due to the observation spikes. (In general, a homogeneous covariance matrix in spectral space decreases rapidly with increasing wavenumber.) In Eq. (9) the observation term is multiplied with the $\mathbf{A}$ matrix, which suppresses the high-wavenumber oscillations, leading to a much smaller increase in J in the next iteration due to the background term. With the above expressions the cost function decreases rapidly and monotonically as a function of the iteration number. After 3 iterations the norm of the gradient has typically decreased by about a factor of 5, and after 15 iterations by a factor of 40. In the assimilation runs the minimization is usually stopped after 15 iterations, with an additional check on the size of the gradient.

The choice of the assimilation time window T depends on both the model and the structure of the measured data. GOME scans the earth in one day, but because of the swath width of 960 km a global coverage (apart from the polar caps) is obtained in roughly three days. As assimilation window we use $T = 24$ h. This choice is motivated as follows. In order to profit from the 4D-Var approach the time interval should be at least several hours. In this way measurements in neighboring orbits are analyzed simultaneously, leading to a smoother and more realistic field in between the orbits. The off-line analysis error is improved due to the inclusion of future observations, as is explained in the sections below. For short time intervals, artificial structures appear in the field with shapes reflecting the GOME swathes. In one day, GOME circles the earth once, and an accurate analysis can be made of the ozone field for a 24-h interval. We tested longer time intervals, but both the forecast and analysis error increase rapidly with increasing assimilation window, due to the neglect of the model error term. For shorter windows the forecast error shows no significant dependence on the window length.

The advantage of the 4D-Var approach is the absence of an explicit time-dependent covariance matrix. In this way the storage and computational costs of running the assimilation scheme are very low compared to full Kalman filtering. Data assimilation becomes feasible for a control variable dimension N of the order of 10^4–10^6. The storage consists of just a couple of field vectors of size N, instead of a matrix of size N^2. Also the number of model iterations is reduced by N. Note that, on the time interval $[0, T]$, the error propagation is correctly treated by the 4D-Var approach, and 4D-Var is equivalent to the Kalman smoother given the same boundary conditions (for linear, unbiased problems with Gaussian error distributions).

At the same time, the disadvantage of 4D-Var is the absence of an explicit covariance matrix. This means that no direct information about the analysis error and correlations is available from the 4D-Var analysis. An alternative approach is needed to estimate and/or propagate the covariances. This is discussed in section 5 for the total ozone assimilation problem.

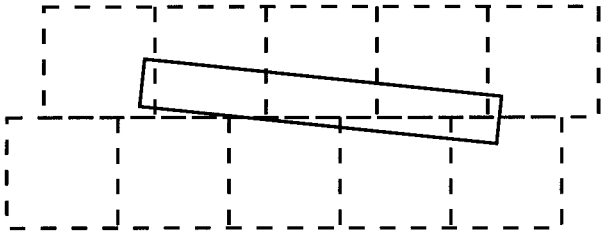

FIG. 2. The 40×320 km^2 GOME pixel has an overlap with several model grid cells.

3. GOME total ozone

The Global Ozone Monitoring Experiment on board the European polar orbiting satellite *ERS-2* measures the spectrum of solar radiation scattered from the earth's atmosphere between 240 and 790 nm, with a resolution of 0.2–0.4 nm. GOME is a nadir-viewing instrument. Total ozone columns are retrieved from the spectra by the GOME Data Processor, which uses the differential optical absorption spectroscopy (DOAS) technique. The result is a slant column ozone density, the amount of ozone along the path of the light. A radiative transfer model is used to calculate the airmass factor. Dividing the slant column by the airmass factor leads to an estimate of the vertical ozone column. GOME has a footprint of 320×40 km^2, shown schematically in Fig. 2. The observation operator $\mathbf{H}_m$ consists of taking the sum of the ozone values in the grid cells overlapping the GOME pixel, weighted by the overlap area. The GOME swath is three pixels wide.

Comparison of GOME-retrieved ozone values with ground-based ozone experiments demonstrates the high accuracy that can be obtained from the instrument combined with the DOAS retrieval. Comparisons with Brewer values show a standard deviation of the order of 4%, but part of this may be caused by time–space differences between the two measurements. The random error, correcting for this representativeness mismatch, is estimated by Piters et al. (1997) to be of the order of 6 Dobson units (DUs) or smaller (about 2%). Apart from this error estimate by validation, the DOAS procedure gives an error related to the precision of the fit to the experimental spectrum. Normally this is much smaller than 6 DU. We used $\sigma_{\text{obs}} = 6$ DU in the assimilation runs, except when the DOAS error is larger, in which case the latter is used as an estimate of the random experimental error. The retrieved GOME pixels are assumed to be uncorrelated, and therefore the matrix $\mathbf{O}$ in Eq. (1) is diagonal (see also section 5).

4. The advection model

As discussed in the introduction, we use a 2D model to advect the ozone columns, using a wind field at a single pressure level (Levelt et al. 1996). This model is simple and convenient for the analysis of total-column tracer data. With the 2D model the problem concerning the height assignment of the total ozone mismatches to the various vertical layers is simplified. Consequently, the 2D wind field will only approximately describe the full 3D transport.

The 2D model is based on a few assumptions. (i) The chemical processes are slow compared to the dynamical redistribution of ozone and a characteristic timescale for the assimilation. The latter two timescales are of the order of 1 day, while the photochemical lifetime of ozone in the lower stratosphere is of the order of months: ozone at these altitudes behaves like a passive tracer. (ii) The transport of ozone is dominated by horizontal advection. We estimate that a vertical transport term in an equation for the total column is, on average, about twice as small as the zonal or meridional term. Note, however, that this number cannot be related directly to the model errors in the global field, since vertical motions are often small scale, and may partly average out. [For a discussion of the importance of vertical motion see, for instance, Riishøjgaard et al. (1992).] (iii) The total ozone variability is dominated by a relatively thin vertical layer. Note that not the ozone maximum but the layer with the maximum temporal variability in ozone determines the fluctuations in total ozone. It was found by Levelt et al. (1996) that the 200-hPa winds minimize the forecast error (for the case of April 1992). This is consistent with the maximum variability assumption and most of the changes in ozone occuring around the tropopause.

Given the above assumptions we are left with a simple linear 2D advection model, described by the following continuity equation:

$$\frac{\partial \Sigma_{O_3}}{\partial t} = -u_0 \frac{\partial \Sigma_{O_3}}{\partial x} - v_0 \frac{\partial \Sigma_{O_3}}{\partial y}. \tag{10}$$

The increase in the ozone column field Σ_{O_3} is determined by the 2D lat–long wind field $\mathbf{v}$ and the 2D gradient of the ozone field.

The wind field is taken from the ECMWF archive. The 6-h forecast, or first guess, horizontal wind fields of a single pressure level are used with a resolution of 1° by 1°, and they are interpolated to the model grid and the model time. These wind fields are available every 6 h. The model grid consists of nearly square grid boxes of roughly 100 × 100 km. In the latitudinal direction the grid points are 1° apart (181 latitude values), and in the longitudinal direction the number of grid boxes is equal to 360 × cos(ϕ), where ϕ is the latitude, ending with a single grid box at $\phi = \pm\pi/2$. The total number of lattice points is 41 258. This is also the dimension of the control variable in the cost function.

Two numerical schemes to solve Eq. (10) have been implemented. The upwind approach was described in Levelt et al. (1996). The results described in this paper are obtained using a semi-Lagrangian (SL) scheme (Robert 1981). Equation (10) is written as

$$\Sigma_{O_3}(\mathbf{r}, t + \Delta t) = \Sigma_{O_3}(\mathbf{r} - \mathbf{v}\Delta t, t). \tag{11}$$

If $\mathbf{r}$ is taken to coincide with one of the lattice points, then $\Sigma_{O_3}(\mathbf{r} - \mathbf{v}\Delta t)$ can be estimated from the model grid values of ozone (the vector $\mathbf{x}$) by interpolation. This value is calculated using third-order interpolations, involving 16 grid points. The scheme does not conserve ozone, but the ozone loss turns out to be small and does not present a problem. The adjoints of the advection routines, needed for the calculation of the gradient in the 4D-Var approach, were written using the adjoint model compiler TAMC (Giering and Kaminski 1998).

The disadvantage of the first-order upwind scheme is its large diffusion. Sharp features are considerably smeared out in a few days. This is greatly improved using the SL approach, which conserves the dynamical range of ozone values over much larger time spans.

In the SL code a few switches occur to prevent oscillations to build up during the advection. This makes the numerical implementation of the model nonlinear and even nondifferentiable. As mentioned before [Eq. (4)], this implies that the linearized model and the adjoint are both functions of the ozone field. This field has to be stored on disk for all time steps in the interval [0, T] in order to be able to calculate the adjoint field. However, this nonlinearity in the SL code is very weak. Therefore, we used the linearized version of the SL routine to construct the adjoint $\mathbf{L}^T$, and the storage of fields is no longer needed. We carefully studied the performance of this construction, using the standard adjoint checks: the gradient test, $\nabla J \cdot \Delta\mathbf{x} \stackrel{?}{=} J(\mathbf{x} + \Delta\mathbf{x}) - J(\mathbf{x})$; and the adjoint test, $\langle \mathbf{x}; \mathbf{L}\mathbf{y} \rangle \stackrel{?}{=} \langle \mathbf{L}^T\mathbf{x}; \mathbf{y} \rangle$ (Huang and Yang 1996). Deviations from the real adjoint are small, typically of the order of 0.1%, and do not significantly influence the minimization.

Figure 3 shows an example of the model forecast performance. A free model run is compared with GOME total ozone measurements, and the globally averaged root-mean-square (rms) of the innovation numbers is plotted. Two numerical advection schemes are compared, using the same starting ozone distribution and wind fields. In the ''no-wind'' reference run the ozone distribution is kept fixed. After one day the model error is about 20 DU. This will consist of model, representativeness, and measurement errors. After the second day there is no evident growth of the error for the SL case for a period of about two weeks. A comparison of figures of assimilated and free model run ozone fields shows that, although there are quantitative local differences, the overall large-scale patterns in the free model run field show a correspondence with the analyzed fields in the first 1–2 weeks. After this initial period the field

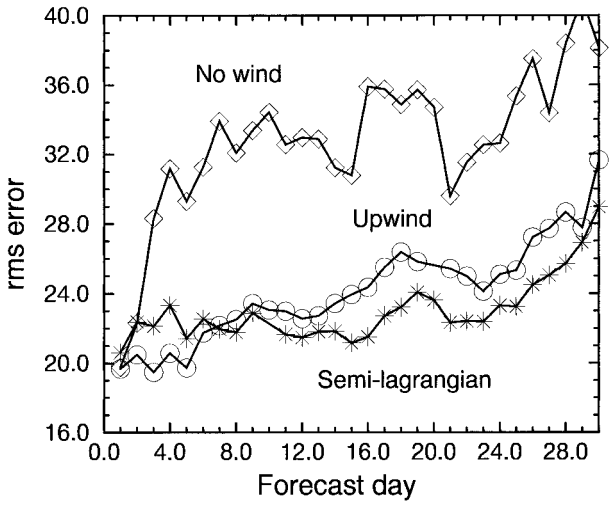

FIG. 3. Increase of the root-mean-square model-GOME deviation, starting from an analyzed field at day 0. The semi-Lagrangian scheme is compared with upwind advection and with a fixed ozone field. Period: 1–31 Mar 1997.

becomes more homogeneous, due to mixing and numerical diffusion, and the error starts to increase.

In the first few days the diffusive upwind scheme performs a few Dobson units better than the SL scheme for this particular run. On average, the upwind and semi-Lagrangian schemes show a very similar forecast skill during the first few days. The sharp gradients in ozone are better conserved in the SL scheme but are sometimes slightly displaced in the 1-day forecast compared to the analysis. The absence of sharp gradients in the upwind scheme forecast results in the absence of error variance on the smaller scales, and therefore a better rms forecast score in those cases. After a few days the large-scale error in the upwind run increases (due to the diffusion), and the SL fields compare better with the measurements.

In the assimilation runs the SL advection scheme is used. This scheme gives a better, more detailed description of the ozone minima and maxima and, correspondingly, a more realistic ozone distribution than the first-order upwind scheme. The SL advection descibes the range in ozone values better when no observations are available (near the poles).

5. Covariance modeling

Apart from deriving a global ozone field from the model and the GOME measurements, it is important to have a reliable estimate of the errors involved. The spatial error distribution will be far from homogeneous: on a GOME swath measured just half an hour ago the error in the analyzed ozone field is considerably smaller than the error of a parcel of air observed two days ago due to the model error growth. Furthermore, at the equator the field is fairly homogeneous and model errors are much smaller than at midlatitudes and in the polar regions. Another important aspect is the correlation between errors. When a model grid point shows a positive forecast field deviation, then the field at neighboring grid points, within a correlation radius, is most likely also too large and should obtain a correction in the analysis procedure as well.

With this in mind the forecast covariance matrix $\mathbf{B}$ is modeled as a product of a homogeneous correlation matrix $\mathbf{F} = \mathbf{A}^2$ and a position- and time-dependent variance field described by a diagonal matrix $\mathbf{D}$, $\mathbf{B} = \mathbf{ADA}$. The variance and correlation matrices are discussed separately below.

The 4D-Var assimilation does not calculate the explicit form of the covariance matrix at the end of the time interval $t = T$. This propagation of the error structure from time $t = 0$ to $t = T$ will be estimated by a separate foreward model run, as described below. A sequential approach is used that does not start directly from the 4D-Var equations. In contrast to the 4D-Var analysis of the field, the model error term is explicitly included in this error analysis procedure. The aim of this combined procedure is to analyze the ozone field as accurately as possible, making use of the advantages of the 4D-Var method, and at the same time to obtain a realistic estimate of the accuracy of these model ozone values.

a. Correlations

For computational convenience we will assume the horizontal error correlations to be homogeneous (and isotropic). The multiplication with the matrix $\mathbf{A}$ (the square root of the correlation matrix $\mathbf{F}$) occurring in Eqs. (8) and (9) is then conveniently calculated by first transforming the field to spectral space. Since $\mathbf{A}$ is diagonalized by this transformation, the matrix product is now a simple multiplication of each spectral component with the corresponding eigenvalue of $\mathbf{A}$.

The covariance radius and the shape of the decay of the correlations are estimated from the forecast departures ($d_i \equiv \mathbf{H}_i\mathbf{x}_{t_i} - y_i$):

$$\mathbf{F}(|\mathbf{r}_i - \mathbf{r}_j|) \approx \frac{\langle d_i d_j \rangle}{\sqrt{\langle d_i^2 \rangle \langle d_j^2 \rangle}}. \tag{12}$$

Note that this expression contains the sum of forecast and measurement errors. The average is over pairs of measurements (i, j) the same distance $r = |\mathbf{r}_i - \mathbf{r}_j|$ apart. We used only measurements in the same time step to evaluate the products $d_i d_j$. This time step is 30 min in the case of SL advection, and in this period the satellite travels about 12 000 km. Note that the GOME data used to evaluate $\mathbf{F}$ are later used in the assimilation. The assumed shape of $\mathbf{F}$ used in the assimilation will slightly influence the estimated $\mathbf{F}$. These dependencies may introduce errors in the calculation.

The correlation as a function of the distance between the measurements is plotted in Fig. 4, using the GOME

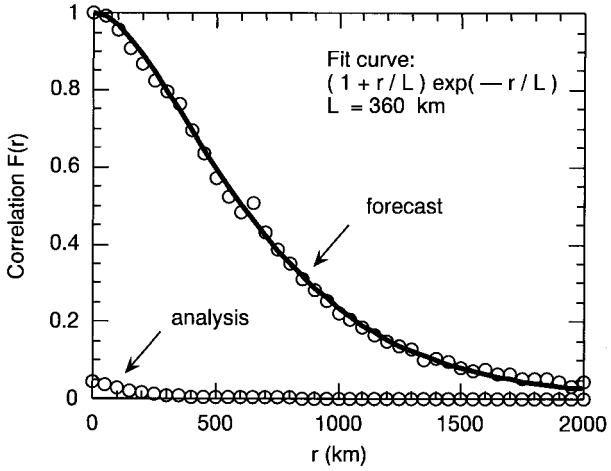

FIG. 4. The correlation F as a function of the distance r between the measurements. The line is a one-parameter fit. The lower curve shows the analysis minus observation covariance, normalized by the forecast minus observation variance.

total ozone data of March 1997. The correlation shows a roughly exponential decay, except for the first 300–400 km. A reasonable fit (dashed line) is obtained using the functional form $F(r) = (1 + r/L) \exp[-r/L]$, $L =$ 360 km. This function was derived by Thiebaux (1976) from the assumption that the errors can be represented as a second-order autoregressive process.

In general, the model and observation covariance will show a different functional behavior. When measurements are uncorrelated in space, the total covariance will consist of a sharp peak at zero distance on top of a broad forecast covariance. In this idealized case the forecast error contribution to the total mismatch can be estimated as the extrapolation of the broad feature to zero distance. The remaining error is then attributed to the observations. In our case, however, there is no clear sign of two features in the forecast minus observation correlation. There may be several reasons for this. First, the dependence of the retrieval on clouds (coverage and heights) and albedo (snow, ice, sand), as well as the use of a priori climatological data in the retrieval, may well cause significant spatial correlations in the total ozone errors with large scales, making it more difficult to separate this from the forecast error term. Second, the spatially uncorrelated random noise of the retrieved GOME total ozone values is estimated to be much smaller than the model forecast error (Piters et al. 1997, 1998). We will therefore use the functional form in Fig. 4 as an approximation to the forecast correlations.

The analysis minus observation covariance provides additional information about the performance of the assimilation scheme (Hollingsworth and Lönnberg 1989). The result is also plotted in Fig. 4. The analysis data are plotted using the normalization factor of the forecast statistics, the denominator in Eq. (12). The correlation length (half-width, half-maximum) is about 140 km for the analyzed field (600 km for the forecast field). The model-measurement mismatches are reduced by more than a factor of 4 by the analysis. This again demonstrates the small uncorrelated random error component in the retrieved observations.

In the discussion of Hollingsworth and Lönnberg an ''efficient'' analysis system is defined as one that leads to negative correlations after the analysis, in which case the field fits the data well. In our case the analysis errors are small, but the correlations remain positive. Note that the discussion about efficiency is based upon the assumption of uncorrelated observation errors, while the GOME total ozone values may well be correlated. GOME provides a very dense set of measurements, with a distance of 40 km between the pixels along the track. The effective resolution of the assimilation system is a few grid cells, and the smallest-scale features along the tracks will not be resolved. Keeping this in mind, an analysis performance with a resolution of about 100–200 km is quite satisfactory.

b. *Error field*

The correlation matrix is kept fixed during the assimilation run, but the diagonal part $\mathbf{D}$, or the error field, is continuously recomputed. After the iterative minimization of the cost function using the 4D-Var approach, the variance field is estimated in a separate integration from time $t = 0$ to time T. This forward integration of the error involves advection of the variance, a model error increase every time step, and a replacing of the forecast error by an analysis error when a measurement occurs. The variance thus obtained at time T determines the new matrix $\mathbf{B}$ for the next assimilation interval. An additional backward integration is used to estimate the analysis error at any time t inside the assimilation interval. The various ingredients are discussed below.

In a Kalman filter approach (Jazwinski 1970) the covariance matrix is recomputed every time step using the following recipe:

$$\mathbf{B}_{t+1} = \mathbf{L}\mathbf{B}_t\mathbf{L}^{\mathrm{T}} + \mathbf{Q}, \tag{13}$$

where $\mathbf{L}$ is again the linearized model, and $\mathbf{Q}$ is a model error term, added every time step. The first term on the right shows that the error covariance is transported by the model, similar to the ozone transport itself. For the tracer advection equation this is intuitively clear: the uncertainty in ozone is a property of a parcel of air and this parcel is transported by the wind field. Unfortunately, it is prohibitively expensive to compute all the matrix elements. As an approximation to this covariance transport, we apply the advection equation $\mathbf{M}$ to the error field σ, $D_{ij} = \delta_{ij}\sigma_i^2$:

$$\alpha_{t+1} = \mathbf{M}[\sigma_t]. \tag{14}$$

For a discussion on the evolution of forecast error covariances, see, for instance, Cohn (1993).

The error field is not only transported, but it will also

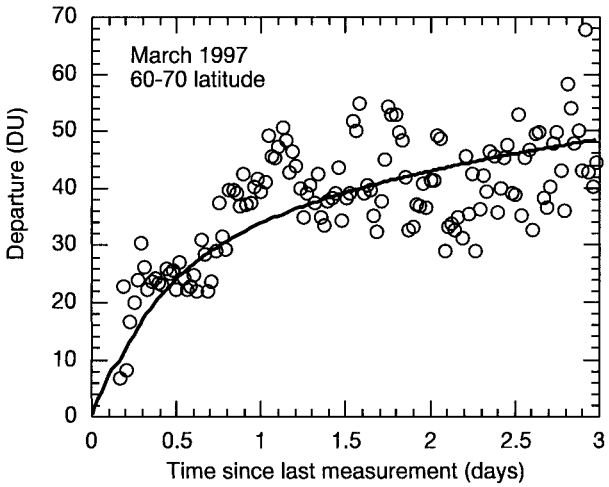

FIG. 5. Model–measurement mismatch plotted against the time field interpolated to the measurement position. Data are accumulated for Mar 1997 and for latitudes between 60° and 70°N. The line shows the one-parameter fit used to model the error increase with time.

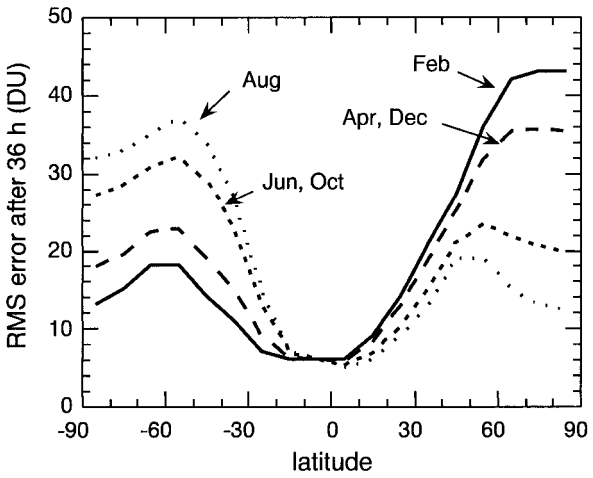

FIG. 6. Modeled season and latitude dependence of the error growth.

grow in time as indicated by the random model error term **Q** in Eq. (13). This error growth can be estimated using the forecast errors. A ''time field'' is introduced, which is advected in the same way as the ozone and error fields. At every time step this field is incremented by 1 in every grid box. When the GOME instrument observes ozone belonging to a certain grid box and the measurement is analyzed, the time field is reset to 0 at that position. A plot of the forecast error versus the time field defined in this way gives an estimate of the error growth with time. An example of the forecast minus observation error statistics is shown in Fig. 5. The figure shows a strong increase in the error in the first 36 h, but then the error saturates (see also Fig. 3). Plots for other latitudes ϕ show a similar behavior with a crossover after about 1 day. We model the behavior by a one-parameter curve. For small times the covariance is assumed to grow linearly with time with a large slope. After a day this rapid increase is smoothly turned into a slow linear increase for large times. Note that the data points are very scattered. This is the case for all plots and the curve is just a crude approximation of the real error. The single parameter $c(\phi)$ is defined as the total error after 36 h. The example shown is one of the largest error increases observed. For other seasons and latitude bands the error is generally smaller. Note that in reality the departure will not go to zero for small time intervals between measurements, as the drawn curve seems to suggest. In the assimilation scheme only the slope of the curves is used to calculate the error increase in a grid box as a function of the previous value of σ_i in that grid box.

If model errors are completely uncorrelated with time, Eq. (13) predicts a square root dependence of the error with time. However, it is reasonable to assume that errors for successive time steps are similar in both magnitude and sign. In the fully correlated case the error growth is linear. On the other hand, in nonlinear models small perturbations will grow exponentially, or $d\sigma/dt$ is proportional to σ for small σ. Unfortunately, the data as shown in Fig. 5 are too noisy to discriminate between these three functional forms, but a linear growth as used in Fig. 5 seems a reasonable choice [see Savijarvi (1995) and references therein].

The error plots and the corresponding parameters $c(\phi)$ are strongly latitude and season dependent. Therefore, we collected data for various months and in 10°-latitude bands. The errors found are large at midlatitudes and around the poles, and much smaller at the equator. The yearly oscillation is described approximately by the following form:

$$c(\phi) = \frac{1}{2}c_{\text{aug}}(\phi)\left[1 + \cos\left(2\pi\frac{m-8}{12}\right)\right] + \frac{1}{2}c_{\text{feb}}(\phi)\left[1 + \cos\left(2\pi\frac{m-2}{12}\right)\right]. \quad (15)$$

Here m is the month, $m \in [1, \ldots, 12]$, and the 36-h error is written as a function of the latitude-dependent error in August and February. This is shown in Fig. 6. The figure shows a striking similarity to the behavior of the climatological annual ozone variation (Whitten and Prasad 1985). The relative error, that is, the model forecast error divided by the natural variability, is more homogeneous.

When a measurement occurs the forecast errors are replaced by analysis errors as a result of the assimilation process. We use a simplified Kalman filter equation to estimate these analysis errors at the time of the measurement.

One of the Kalman filter equations describes the reduction of the covariances when a new set of observations is analyzed:

$$\mathbf{A} = \mathbf{B} - \mathbf{B}\mathbf{H}^{\mathrm{T}}[\mathbf{O} + \mathbf{H}\mathbf{B}\mathbf{H}^{\mathrm{T}}]^{-1}\mathbf{H}\mathbf{B}. \quad (16)$$

Here the analysis and forecast covariances **A** and **B** are defined on the model grid, **O** has a dimension equal to the number of observations, and **H** interpolates the model field to the measurement positions. When the interpolation matrix **H** is generalized by including a ''time interpolation'' as well [e.g., Eq. (6)], then this formula also applies to the analysis covariance of the 4D-Var (Lorenc 1988).

To understand the implications of this equation, consider a grid point at a distance r from a group of n measurements centered at an origin 0. Assume that the distances between the measurement points are small compared to r and are shorter than the forecast covariance radius. For this situation the term $\mathbf{B}\mathbf{H}^{\mathrm{T}}$ will assign almost equal weights to all the measurements. When **O** and **B** are assumed to be roughly homogeneous, these matrices can be replaced by $m\sigma_{\mathrm{obs}}^2$ and $n\sigma_b^2$, respectively. A second number, m, is introduced as the average number of measurements inside a circle with a radius determined by a measurement covariance length (similarly, n is the number of measurements within a forecast covariance radius). In other words, m is related to the average number of correlated measurements. Writing the covariance as a product of a distance-dependent correlation function and local forecast errors,

$$\sigma_a^2(\mathbf{r}) \approx \sigma_b^2(\mathbf{r}) - F(r)\sigma_b(\mathbf{r})\sigma_b(0)\frac{n}{m\sigma_{\mathrm{obs}}^2 + n\sigma_b^2(0)}F(r)\sigma_b(\mathbf{r})\sigma_b(0). \quad (17)$$

When $m\sigma_{\mathrm{obs}}^2 \ll n\sigma_b^2$, the following simple approximate formula is obtained:

$$\sigma_a^2(\mathbf{r}) \approx [1 - F^2(r)]\sigma_b^2(\mathbf{r}) + F^2(r)\sigma_b^2(\mathbf{r})\frac{m\sigma_{\mathrm{obs}}^2}{n\sigma_b^2(0)}. \quad (18)$$

Two important features of the covariance analysis equation are now clear. First, the influence of the measurements $[F^2(r)]$ extends over a distance determined by the forecast correlation length. Far away from the GOME swath $F \approx 0$ and $\sigma_a \approx \sigma_b$. On the GOME track $F \approx 1$ and $\sigma_a \sim \sigma_{\mathrm{obs}}$. Second, the observation variance is reduced by the prefactor m/n. This prefactor is related to the ratio of the correlation lengths of the forecast and observation errors and may be interpreted as a grouping of GOME measurements into ''superobservations'' with a reduced observation error. We assume that the observation covariance radius is smaller than the forecast covariance radius, which implies $m/n < 1$. Unfortunately, we do not have a quantitative guess of the correlations between the GOME measurements. However, the estimated forecast error field, a combination of analysis and model errors, is mainly determined by the error growth described above, as long as $m/n < 1$ and/or the observations are accurate. Therefore, the forecast error estimate is not very sensitive to the choice of m/n.

The sequential error estimate described above accounts only for the influence of past measurements on the error field. In the 4D-Var approach, however, future and past measurements have an equal influence on the analysis. For the total ozone assimilation we want a realistic estimate of the error at all times t_0 in the assimilation window $[0, T]$. The error due to past measurements, σ^p, is estimated using the procedure described above, by advecting the error field, adding a forecast error increment every time step, and replacing the forecast error by an analysis error when a measurement occurs. For the set of future measurements with $t > t_0$, σ^f at $t = T$ is initialized to a large value reflecting the natural variability in ozone. This error field is advected backward in time by changing the sign of the wind fields. Every negative time step a forecast error increment is added and the analysis [Eq. (18)] is used near measurement positions. The estimated error field is obtained from a combination of these two error fields at $t = t_0$:

$$\frac{1}{\sigma^2} = \frac{1}{(\sigma^p)^2} + \frac{1}{(\sigma^f)^2}. \quad (19)$$

This means that the ozone field is considered as resulting from independent future and past assimilation runs with local Gaussian errors σ^f and σ^p. The resulting error estimate is smaller than either σ^p or σ^f.

The error-modeling procedure described above provides a forecast error estimate at any position and time, also when no observations are available. We checked the approach a posteriori by plotting the predicted error field versus the observed forecast-minus-measurement innovation numbers. The results are quite satisfatory. Although there are some oscillations, the data points on average follow a straight line with slope 1.

6. Assimilation results

In Fig. 7 the GOME tracks of 9 March and the corresponding assimilated ozone field are shown. For comparison we also show the accumulated Advanced Earth Observing Satellite (ADEOS) TOMS total ozone field made available by NASA. One prominent difference between GOME and ADEOS–TOMS is the swath width. For GOME this is relatively narrow, while the TOMS swaths are wide, covering the globe in 1 day. The GOME and TOMS pictures are 24-h composites; that is, the columns of 24 h of measurements are all plotted in the same figure. Because ozone transport is not taken into account, a mismatch occurs at the date line (180° longitude), where the time difference between the tracks is about 24 h.

The assimilated ozone field is shown for $t = 1200$ UTC, and the assimilation time window is from $t = 0000$ UTC to $t = T = 2400$ UTC. The field is only plotted when the estimated error is smaller than 25 DU. We choose to plot the field at $t = T/2$, because in this case the analysis is influenced by 12 hours of past mea-

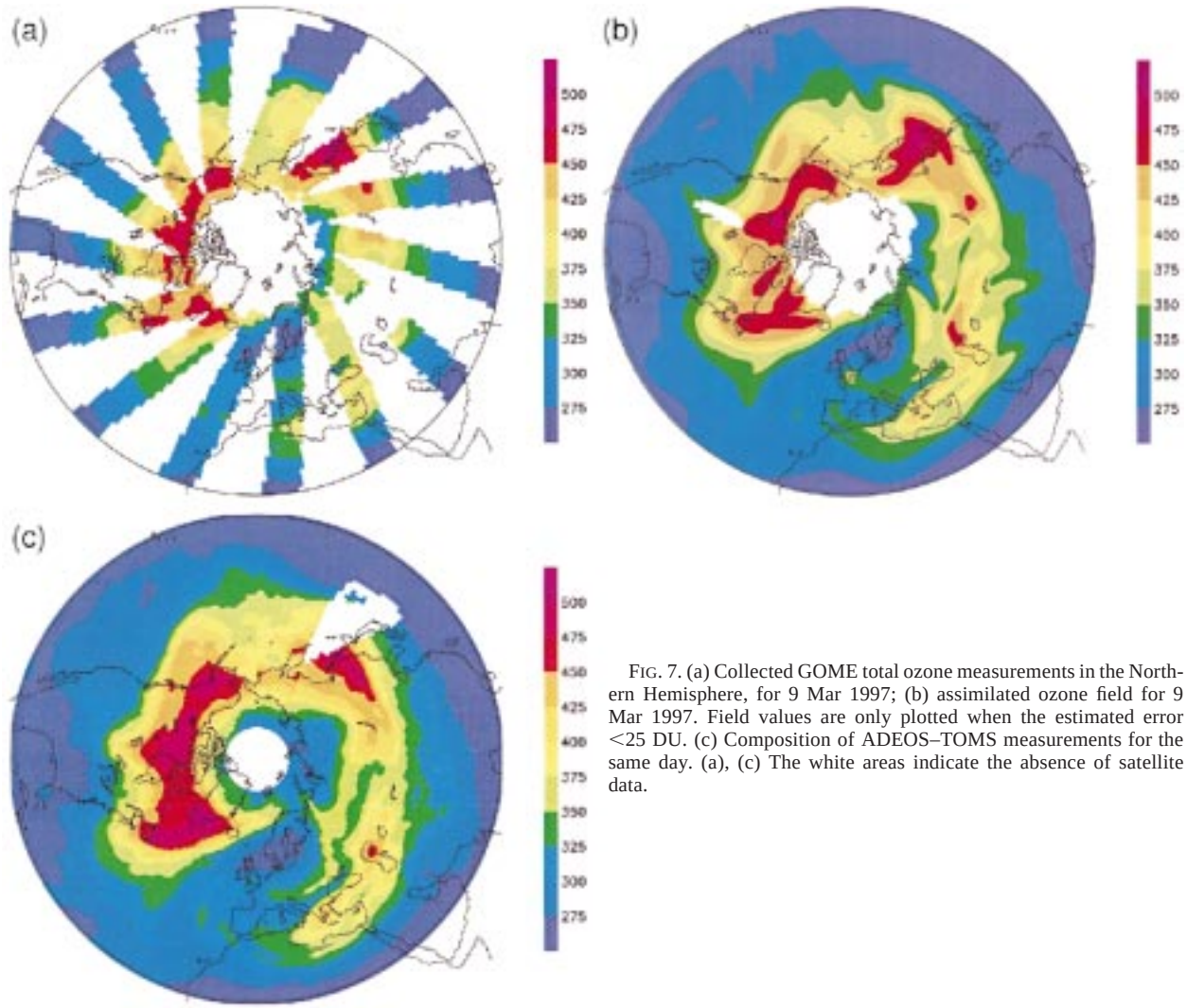

FIG. 7. (a) Collected GOME total ozone measurements in the Northern Hemisphere, for 9 Mar 1997; (b) assimilated ozone field for 9 Mar 1997. Field values are only plotted when the estimated error <25 DU. (c) Composition of ADEOS–TOMS measurements for the same day. (a), (c) The white areas indicate the absence of satellite data.

surements and 12 hours of future measurements, resulting in an accurate description of the ozone field. Note that at $t = 12$ the satellites are approximately flying at 0° longitude. The field in the lower half of the picture therefore closely matches the measurements, while in the field in the upper half, displacements occur due to almost 12 hours of transport.

The figure demonstrates the added value of data assimilation: with an upper boundary for the error of 25 DU most of the large areas without GOME data are filled in and the result is an almost global ozone field with a realistic uncertainty at any moment required.

There is an interesting data void in the track above Kazakhstan, 45°N, 60°E. The assimilated field predicts a peak in ozone at this spot although no trace of a peak is found in the GOME data of 9 March. This peak is the result of GOME observations of previous days, transported by the wind to this location. That this ozone peak is realistic is demonstrated by the TOMS data.

Another interesting feature of the ozone field of 9 March are the low ozone values above Scandinavia and Scotland. The assimilated result shows that this is a large intrusion of midlatitude air into the polar vortex, with ozone values almost a factor of 2 lower than above northern Canada. Note that especially the ozone values above 450 DU are higher in the case of TOMS compared to GOME. This is a difference between the DOAS retrieval for GOME and the TOMS-retrieved ozone values, and may be related to the albedo (snow) and the high solar zenith angles.

The early stage of the ozone hole is shown in Fig. 8. On 11 September the sun is about to reappear at the South Pole. The ozone hole has already formed but the UV/visible GOME spectrometer observes only the outer rim on the South America side of the globe. The 4D-Var assimilation is nevertheless able to reconstruct the hole from the low ozone values at the end of the tracks. The measured low ozone spots are connected smoothly

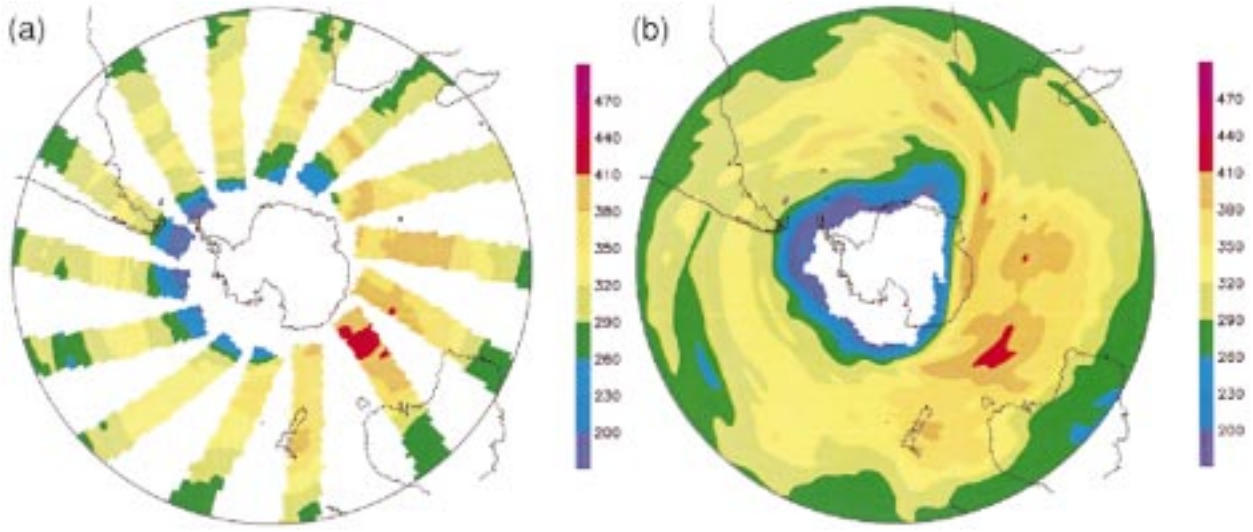

FIG. 8. (a) Collected GOME total ozone measurements in the Southern Hemisphere, 11 Sep 1996; (b) assimilated ozone field for the same day. Field values are plotted when the estimated error <30 DU.

and form a ring of total ozone values below 200 DU. In the center of the hole there is still a hump of high ozone values. There are no measurements available here, and since the model does not account for chemistry, the only way that these higher values can disappear is by means of transport away from the pole. Before, we chose the 200-hPa wind field to advect total ozone. However, for the Antarctic ozone hole the variability due to the heterogeneous chemistry occurs predominantly around the ozone maximum. Therefore, we use 50-hPa winds in the period when the ozone hole is present.

The effect of the 4D-Var method on the estimated error is shown in Fig. 9. The error distribution is compared with an error that would approximately result from a sequential data-assimilation scheme, such as optimum interpolation, in which only past measurements are incorporated in the analysis. This latter error estimate is obtained by running the simplified error estimate, described in the previous section, foreward in time until 1200 UTC. Since 12 hours of future data are included in the 4D-Var analysis at 1200 UTC, the reliability of the field, especially west of the position of the current orbit of the satellite, has improved considerably. The efficient way of using both past and future data (in an off-line data analysis) is an important advantage of the 4D-Var approach over sequential data-assimilation methods.

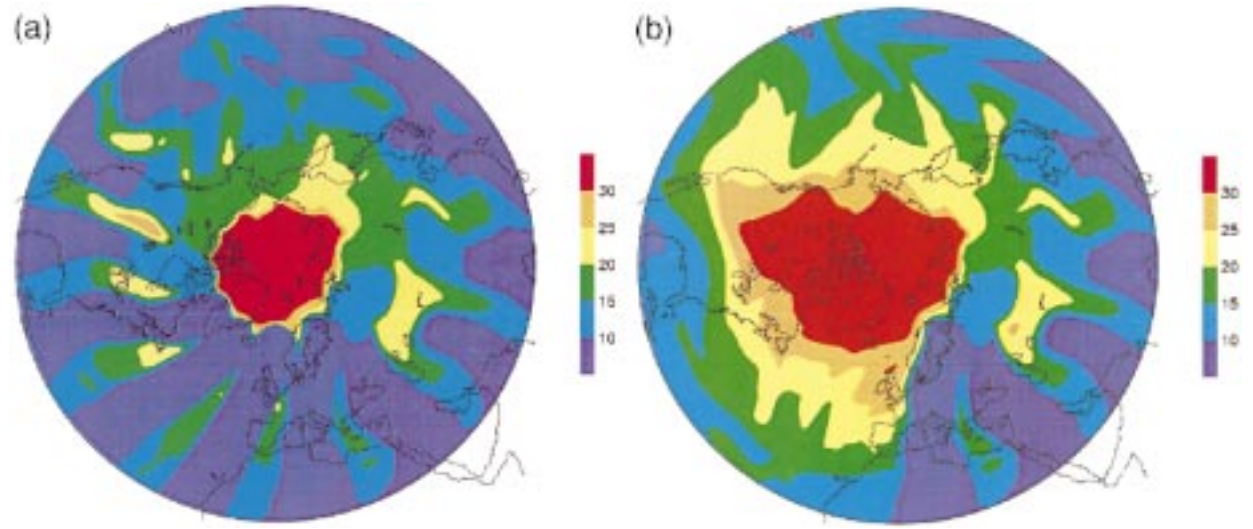

FIG. 9. The estimated error field (a) halfway through the 4D-Var time interval of 24 h, compared with the similar error estimate (b) for a sequential data-assimilation technique where only past measurements are accounted for; 1200 UTC 9 Mar 1997.

7. Conclusions

In this paper we presented a detailed description of an assimilation scheme for global total-column ozone satellite data. The advection model transports O_3 columns using a 2D (lat–long) wind field at a fixed pressure level and on a 100-km horizontal grid. A 4D-variational assimilation scheme with a 24-h time interval is used to assimilate *ERS-2* GOME total ozone retrieved values. The 4D-Var implementation as described in section 2 shows a fast convergence. The analysis and covariance computations for one day of GOME data take about 20 min on an average modern workstation without excessive memory demands.

In 4D-Var the evolution of the error covariance is implicitly taken into account, but no explicit covariance matrix appears in the algorithm. Due to the spatial and temporal distribution of measurements from an instrument like GOME, the forecast error is largely inhomogeneous and the distribution of errors is strongly time dependent. Because of this the error modeling requires special attention. The covariance matrix is written as a product of a homogeneous correlation matrix and an error field depending on both space and time. The corresponding covariance distance dependence, model error growth in time and latitude, and seasonal dependence of the forecast and model errors were determined from the forecast error statistics. As a result, a realistic error bar can be attached to the assimilated ozone columns.

The preconditioned 4D-Var algorithm converges well also in the case of large covariance radii. In this case, minimizing of the forecast–measurement mismatch for one pixel will influence many others. The algorithm has to find the optimal compromise between the rapidly oscillating increments from the measurements and the smooth adjustments demanded by the covariance matrix.

The added value of data assimilation is demonstrated in the previous section. It delivers an almost global ozone field at any time desired. The large data voids in the measurements are filled in by the transport in the model.

The 4D-Var approach has a few advantages over other assimilation schemes. Inside the assimilation window of 24 h all the data are incorporated into a single analysis. Furtheremore, the error correlations become state dependent (as in a Kalman filter) and are partly determined by the model dynamics. These features help to connect the data from neighboring GOME tracks in a smooth and realistic way. This is demonstrated in Fig. 8, showing the September ozone hole. Artificial structures related to the distribution of the measurements (GOME tracks) are found to be reduced compared to the single correction approach. Perhaps the most attractive feature of the variational approach, in the present context of the off-line assimilation of (chemical) tracer observations, is that the information of future measurements is built into the analysis of the fields with $t < T$, in a way that is consistent with the dynamics of the model. Because of this we showed the analyzed fields at $t = T/2$. This efficient use of the data results in a large improvement of the estimated error, as shown in Fig. 9. In some sense up to twice as many measurements are available in the 4D-Var approach as compared to sequential assimilation techniques.

In the present approach we avoided the problem of distributing the forecast–measurement mismatch in the total column over the various vertical layers of a 3D model of the atmosphere. The price we paid is that the model predictions are not very good and the forecast errors increase rapidly with time. This may be expected since all ozone is assumed to be transported horizontally with the same wind field. Probably more important is the neglect of vertical transport. We checked the possibility to improve the 2D model by adding a term that mimics this neglect of vertical motion. The temperature (Stanford and Ziemke 1996) and vertical velocity are possible candidates. However, we did not find a convincing correlation between these variables and forecast error structures.

The 4D-Var total ozone assimilation approach described above is practical and results in an almost global ozone field with an estimated error below 25 DU, despite the simplicity of the model. Due to the relatively high resolution the model can resolve small features present in the GOME data. This makes it a useful tool for the analysis and validation of total ozone satellite data.

Acknowledgments. We acknowledge stimulating discussions with Ad Stoffelen, Elias Hólm, and Ad Jeuken. HE is supported by the Dutch Beleidscommissie Remote Sensing.

REFERENCES

Burrows, J., 1993: Global Ozone Monitoring Experiment, interim science report. Tech. Rep. SP-1151, ESA/ESTEC, Noordwijk, Netherlands, 59 pp. [Available from ESA/ESTEC, Publications Division, P.O. Box 299, 2200 AG Noordwijk, Netherlands.]

Cohn, S. E., 1993: Dynamics of short-term univariate forecast error covariances. *Mon. Wea. Rev.,* **121,** 3123–3149.

Courtier, P., J. Derber, R. Errico, J. F. Louis, and T. Vukićević, 1993: Important literature on the use of adjoint, variational methods and the Kalman filter in meteorology. *Tellus,* **45A,** 342–357.

Daley, R., 1991: *Atmospheric Data Analysis.* Cambridge University Press, 457 pp.

Eichmann, K.-U., K. Bramstedt, M. Weber, V. Rozanov, R. deBeek, R. Hoogen, and J. P. Burrows, 1997: Ozone profile retrieval from GOME satellite data. II: Validation and applications. *Proc. Third ERS Symp.,* ESA-SP 414, Florence, Italy, ESA, 749–758.

Elbern, H., H. Schmidt, and A. Ebel, 1997: Variational data assimilation for tropospheric chemistry modeling. *J. Geophys. Res.,* **102,** 15 967–15 985.

Fisher, M., and D. J. Lary, 1995: Lagrangian four-dimensional variational data assimilation of chemical species. *Quart. J. Roy. Meteor. Soc.,* **121,** 1681–1704.

Giering, R., and T. Kaminski, 1998: Recipes for adjoint code construction. *ACM Trans. Math. Software,* **24,** 437–474.

Gilbert, J. Ch., and C. Lemaréchal, 1989: Some numerical experi-

ments with variable-storage quasi-Newton algorithms. *Math. Progr.,* **45,** 407–435.

Hollingsworth, A., and P. Lönnberg, 1989: The verification of objective analysis: Diagnostics of analysed system performance. *Meteor. Atmos. Phys.,* **40,** 3–27.

Huang, X.-Y., and X. Yang, 1996: Variational data assimilation with the Lorenz model.

Jazwinski, A. H., 1970: *Stochastic Processes and Filtering Theory.* Academic Press, 376 pp.

Jeuken, A. B. M., H. J. Eskes, P. van Velthoven, H. M. Kelder, and E. V. Hólm, 1999: Assimilation of total ozone satellite measurements in a 3D tracer transport model. *J. Geophys. Res.,* **104,** 5551–5563.

Lary, D. J., M. P. Chipperfield, J. A. Pyle, W. A. Norton, and L. P. Riishøjgaard, 1995: Three-dimensional tracer initialization and general diagnostics using equivalent PV latitude-potential-temperatures coordinates. *Quart. J. Roy. Meteor. Soc.,* **121,** 187–210.

Le Dimet, F. X., and O. Talagrand, 1986: Variational algorithms for analysis and assimilation of meteorological observations: Theoretical aspects. *Tellus,* **38A,** 97–110.

Levelt, P. F., M. A. F. Allaart, and H. M. Kelder, 1996: On the assimilation of total-ozone satellite data. *Ann. Geophys.,* **14,** 1111–1118.

Lewis, J. M., and J. C. Derber, 1985: The use of adjoint equations to solve a variational adjustment problem with advective constraints. *Tellus,* **37A,** 309–322.

Lorenc, A. C., 1988: Optimal nonlinear objective analysis. *Quart. J. Roy. Meteor. Soc.,* **114,** 205–240.

Munro, R., R. Siddans, W. J. Reburn, and B. J. Kerridge, 1998: Direct measurement of tropospheric ozone distribution from space. *Nature,* **392,** 168–171.

Piters, A. J. M., P. F. Levelt, and H. M. Kelder, 1997: GOME validation using data assimilation. *Proc. Third ERS Symp.,* ESA-SP 414, Florence, Italy, ESA, 637–640.

——, ——, M. A. F. Allaart, and H. M. Kelder, 1998: Validation of GOME total ozone column with the assimilation model KNMI. *Adv. Space Res.,* **22,** 1501–1504.

Riishøjgaard, L. P., 1996: On four-dimensional variational assimilation of ozone data in weather-prediction models. *Quart. J. Roy. Meteor. Soc.,* **122,** 1545–1571.

——, F. Lefèvre, D. Cariolle, and P. Simon, 1992: A GCM simulation of the northern hemisphere ozone field in early February 1990, using satellite total ozone for model initialisation. *Ann. Geophys.,* **10,** 54–74.

Robert, A., 1981: A stable numerical integration scheme for the primitive meteorological equations. *Atmos.–Ocean,* **19,** 35–46.

Savijarvi, H., 1995: Error growth in a large numerical forecast model. *Mon. Wea. Rev.,* **123,** 212–221.

Stanford, J. L., and J. R. Ziemke, 1996: A practical method for predicting midlatitude total column ozone from operational forecast temperature fields. *J. Geophys. Res.,* **101,** 28 769–28 773.

Talagrand, O., and P. Courtier, 1987: Variational assimilation of meteorological observations with the adjoint vorticity equation. I: Theory. *Quart. J. Roy. Meteor. Soc.,* **113,** 1311–1328.

Thiebaux, H. J., 1976: Anisotropic correlation functions for objective analysis. *Mon. Wea. Rev.,* **104,** 994–1002.

Whitten, R. C., and S. S. Prasad, Eds., 1985: *Ozone in the Free Atmosphere.* Van Nostrand Reinhold, 288 pp.